PHYSICAL REVIEW B **89**, 174416 (2014)

Gilbert damping constants of Ta/CoFeB/MgO(Ta) thin films measured by optical detection of precessional magnetization dynamics

Satoshi Iihama,[1,*] Shigemi Mizukami,[2,†] Hiroshi Naganuma,[1] Mikihiko Oogane,[1] Yasuo Ando,[1] and Terunobu Miyazaki[2]

[1]*Department of Applied Physics, Graduate School of Engineering, Tohoku University, Sendai, Japan*

[2]*WPI Advanced Institute for Materials Research, Tohoku University, Sendai, Japan*

(Received 24 March 2014; published 13 May 2014)

The magnetization dynamics of both Ta/CoFeB/MgO and Ta/CoFeB/Ta films were investigated using an all-optical pump-probe method. The magnetic field strength and the applied field direction dependencies of the precession frequency and the relaxation time were explained well by the Landau-Lifshitz-Gilbert equation when taking the magnetic anisotropy distribution in the film into account. The thickness dependence of the α values obtained for both stacked films was also discussed. The α values increased linearly with increasing inverse CoFeB thickness (t_{CoFeB}). The slope of the α vs $1/t_{\mathrm{CoFeB}}$ characteristic for Ta/CoFeB/MgO films was smaller than that for Ta/CoFeB/Ta films, implying that the enhancement of α was caused by the CoFeB/Ta interface. Comparison of the annealing temperature dependence of α and the perpendicular magnetic anisotropy constant K_{u} revealed no correlation between α and K_{u}.

DOI: 10.1103/PhysRevB.89.174416 PACS number(s): 75.78.−n

I. INTRODUCTION

The spin-transfer-torque magnetoresistive random access memory (STT-MRAM) has attracted considerable attention in the development of nonvolatile memories with low power consumption and high-speed performance. The magnetic tunnel junctions (MTJs) of STT-MRAMs require a high tunnel magnetoresistance (TMR) ratio and perpendicular magnetic anisotropy (PMA), which is necessary for high-density STT-MRAMs. However, investigation of the fast magnetization dynamics is also important because of their effects on both operating speed and power consumption. The magnetization dynamics are generally described by the Landau-Lifshitz-Gilbert (LLG) equation as

$$\frac{d\boldsymbol{m}}{dt} = -\gamma\mu_0\boldsymbol{m}\times\boldsymbol{H}_{\mathrm{eff}} + \alpha\boldsymbol{m}\times\frac{d\boldsymbol{m}}{dt}, \tag{1}$$

where $\boldsymbol{m}$ is the unit magnetization vector, $\boldsymbol{H}_{\mathrm{eff}}$ is the effective magnetic field, and α is the Gilbert damping constant. In Slonczewski's theory, the current density for current-induced magnetization reversal is proportional to both the PMA constant $K_{\mathrm{u}}^{\mathrm{eff}}$ and α, which appeared in the LLG equation [1]; here $K_{\mathrm{u}}^{\mathrm{eff}} = K_{\mathrm{u}} - \frac{1}{2}\mu_0 M_{\mathrm{s}}^2$ and K_{u} is the intrinsic perpendicular magnetic anisotropy constant. To retain information for a long time despite thermal fluctuations, films with higher $K_{\mathrm{u}}^{\mathrm{eff}}$ values are required. To resolve the dilemma between the thermal stability and the reversal current density, it is important to search for low α materials with high PMA. The CoFeB/MgO/CoFeB MTJ has attractive properties for use in STT-MRAMs, because this MTJ shows a high TMR ratio [2,3] and CoFeB thin films exhibit PMA [4], which originates from the interfacial magnetic anisotropy between the CoFeB and MgO layers [5]. There have been many reports on the interfacial PMA between MgO and CoFeB [6–11]. However, there have been few reports on the magnetization dynamics of the PMA CoFeB films. In the case of relatively thick CoFeB films, α has a relatively small value of about 0.004 [12,13]. However, α increased with decreasing CoFeB thickness, which is necessary to achieve PMA. The film with a thickness of 1.2 nm shows $\alpha = 0.027$ [4]. Both PMA and α are related to the spin-orbit interaction [14,15], and therefore there is a possibility that the orbital bonding of the Fe and O atoms enhances both α and PMA. Previously, enhancement of α because of spin-orbit interactions via Co $3d$-Pt $5d$ hybridization at the interface was suggested experimentally in thin Co films sandwiched by Pt layers [16], and a first-principles calculation of α was also reported in the Co/Pd bilayer system [17]. α seems to be expressed as $\alpha = \alpha_{\mathrm{bulk}} + \alpha_{\mathrm{s}}/t_{\mathrm{FM}}$ [17], where α_{bulk}, α_{s}, and t_{FM} are the α values of the bulk and the interface, and the thickness of the ferromagnetic layer, respectively. The spin-pumping effect is also effective in the case where the ferromagnetic layer thickness is sufficiently thin [18]. However, the magnetization dynamics contain extrinsic damping mechanisms other than Gilbert damping, such as inhomogeneous linewidth broadening and/or two-magnon scattering. The α values were mostly evaluated from the angular or microwave frequency dependencies of the ferromagnetic resonance (FMR) spectrum, where their extrinsic contributions can be separated because of their different linewidth behaviors, in contrast with that expected from the LLG equation [19–22]. Previously, we reported on the magnetization dynamics of thin CoFeB/MgO films measured by conventional cavity FMR, and on the time-resolved magneto-optical Kerr effect (TRMOKE) using an all-optical pump-probe method. A small apparent α value of 0.01 was obtained [23] for a 1.2-nm-thick CoFeB film in the TRMOKE experiment because of the high external magnetic field. Basically, a high external magnetic field can suppress any extrinsic contributions to the magnetization dynamics, because the precessional magnetization dynamics are dominated by the external field rather than the inhomogeneous effective field. Practical magnetization dynamics results for thin CoFeB/MgO films using coplanar waveguides [24] and vector network analyzer-FMR measurements [25] have been reported. In these measurements, microwaves of several tens of GHz and external magnetic fields that are higher than those

*iihama@mlab.apph.tohoku.ac.jp
†mizukami@wpi-aimr.tohoku.ac.jp

used for conventional FMR measurements can be applied. Femtosecond laser-induced magnetization dynamics have no frequency limits and higher external magnetic fields can be applied because of the time-domain measurements. Therefore, the TRMOKE measurement has an advantage in the evaluation of α. In this paper, we report a systematic investigation of the intrinsic α values of thin Ta/CoFeB/MgO and Ta/CoFeB/Ta films using high external magnetic fields of up to 2 T using TRMOKE measurements.

II. EXPERIMENT

Samples were fabricated using the ultrahigh vacuum magnetron sputtering method, with a base pressure of less than 1×10^{-7} Pa. The stacked structure is as follows: Si/SiO_2 sub./Ta(5)/CoFeB(t_{CoFeB})/MgO(2)/Al(2) (thicknesses in nm).

Postannealing was performed after the deposition of all films. The annealing temperature (T_a) varied from room temperature up to 350 °C and the annealing time was 1 h. To investigate the interfacial influences between the CoFeB/MgO and CoFeB/Ta interfaces, a Si/SiO_2 sub./Ta(5)/CoFeB(t_{CoFeB})/Ta(5) structure was also fabricated. The magnetic properties were measured using a vibrating sample magnetometer (VSM) and a superconducting quantum interference device (SQUID). The magnetization dynamics were measured by TRMOKE using an all-optical pump-probe method. The laser wavelength, pulse width, and repetition rate were 800 nm, 300 fs, and 1 kHz, respectively. The pump beam was modulated with a frequency of 360 Hz using an optical chopper, and the signal was detected using a lock-in amplifier. The magnetization time dependence was detected via the polar magneto-optical Kerr effect of the probe beam and the Kerr rotation angle was detected by the differential method. All measurements were performed at room temperature.

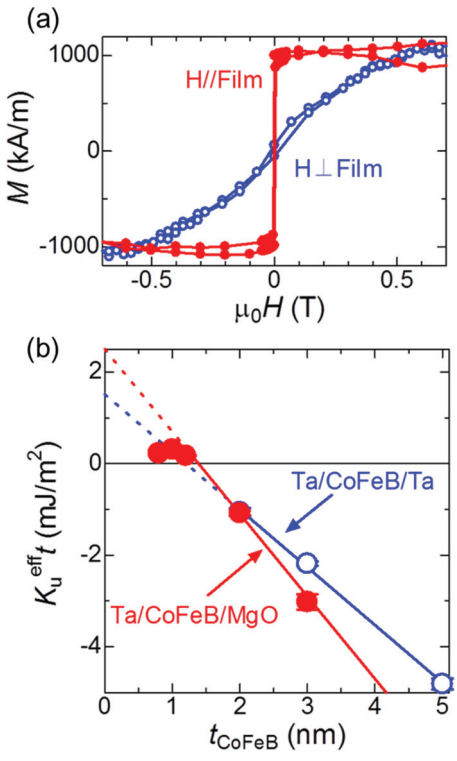

FIG. 1. (Color online) (a) Magnetization curves measured by SQUID for Ta/CoFeB (1.0 nm)/MgO annealed at $T_a = 250$ °C. (b) Products of K_u^{eff} and CoFeB thickness (t_{CoFeB}) as a function of t_{CoFeB} for Ta/CoFeB/MgO (open circles) and Ta/CoFeB/Ta (solid circles). The y intercept indicates the interfacial anisotropy.

III. RESULTS AND DISCUSSION

A. Magnetic properties

Figure 1(a) shows the magnetization curves measured using the SQUID for the Ta/CoFeB(1.0 nm)/MgO structure annealed at $T_a = 250$ °C. The solid and open circles represent the data that were collected with perpendicular ($H \perp$ film) and in-plane magnetic fields ($H \parallel$ film) relative to the film, respectively. The sample clearly shows PMA and the saturation magnetic field is 0.6∼0.7 T. Films with CoFeB thicknesses of less than 1.2 nm exhibited PMA for all annealing temperatures. The products of K_u^{eff} and t_{CoFeB} were plotted as a function of t_{CoFeB}, as shown in Fig. 1(b). The y intercept indicates the interfacial magnetic anisotropy. Both the MgO and Ta interfaces seem to have positive interfacial PMAs, and the interfacial PMA of the MgO interface is larger than that of the Ta interface.

B. Laser-induced precessional magnetization dynamics

Near zero delay time (to within several ps) ultrafast demagnetization occurs, caused by pulse heating by the pump beam. After remagnetization, the precessional motion of magnetization is excited. Figure 2(a) shows the coordinate system used to describe the laser-induced magnetization dynamics. Figure 2(b) shows typical TRMOKE signals for the Ta/CoFeB/MgO structure with $t_{CoFeB} = 1.0$ nm and $T_a = 250$ °C, for which magnetization curves are shown in

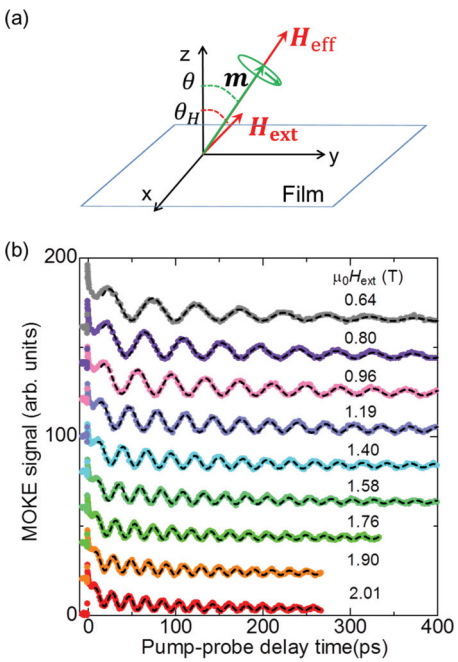

FIG. 2. (Color online) (a) Schematic illustration of the coordinate system used. (b) Typical TRMOKE signals with various external fields H_{ext} measured at a fixed field angle $\theta_H = 70°$ for Ta/CoFeB (1.0 nm)/MgO films annealed at $T_a = 250$ °C.

Fig. 1(a). This film has the highest K_u^{eff} in this paper. The signals were measured with different external magnetic fields (H_{ext}) at a fixed field angle $\theta_H = 70°$, which is the angle between the film normal and the external field, as shown in Fig. 2(a). Precessional damping in the low H_{ext} region looks high compared with that at the high H_{ext} region, which may be caused by extrinsic contributions. The precession frequency and lifetime were evaluated by fitting the experimental data using the following function, which is a summation of the recovery of the magnetization (second term) and the decay of the magnetization precession (third term):

$$\theta_K(t) \sim A + B\exp(-\nu t) + A_0 \exp\left(-\frac{t}{\tau}\right)\sin(2\pi f t + \phi_0), \tag{2}$$

where A, B, and ν are the offset, the demagnetization magnitude, and the recovery rate, respectively. A_0, f, τ, and ϕ_0 are the amplitude, the precession frequency, the lifetime, and the initial phase, respectively.

Figure 3(a) shows the θ_H dependence of both f and $1/\tau$ for the case of a 2.0-nm-thick Ta/CoFeB/MgO film, obtained from a curve fitting at a fixed $\mu_0 H_{ext} = 1.03$ T, at which a sample shows in-plane magnetic anisotropy. Figure 3(b) shows both f and $1/\tau$ as functions of H_{ext} at a fixed $\theta_H = 40°$.

Here, we describe our analysis method derived from the LLG equation. The precession frequency f_{LLG}, the inverse lifetime $1/\tau_{LLG}$ and their field components H_1, H_2 can be calculated while taking the uniaxial anisotropy energy into consideration as [26]

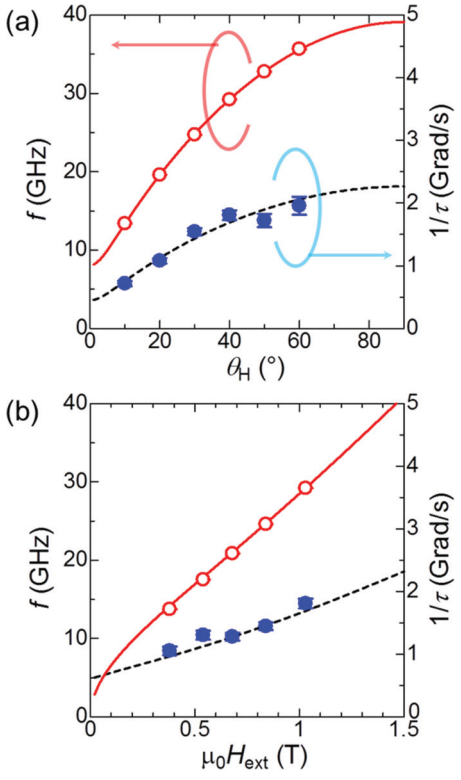

FIG. 3. (Color online) (a) Precession frequency f and inverse lifetime $1/\tau$ measured at various external fields H_{ext} as a function of the field angle θ_H for a Ta/CoFeB (2.0 nm)/MgO film, which shows in-plane magnetic anisotropy. (b) f and $1/\tau$ measured at various values of θ_H as a function of H_{ext}. The solid and broken lines indicate the results of theoretical calculations.

$$f_{LLG} = \frac{\gamma\mu_0}{2\pi}\sqrt{H_1 H_2}, \tag{3}$$

$$\frac{1}{\tau_{LLG}} = \frac{1}{2}\alpha\gamma\mu_0(H_1 + H_2), \tag{4}$$

$$H_1 = H_{ext}\cos(\theta - \theta_H) + H_k^{eff}\cos^2\theta, \tag{5}$$

$$H_2 = H_{ext}\cos(\theta - \theta_H) + H_k^{eff}\cos 2\theta, \tag{6}$$

$$H_{ext}\sin(\theta_H - \theta) - \tfrac{1}{2}H_k^{eff}\sin 2\theta = 0, \tag{7}$$

where H_k^{eff} and γ are the PMA field and the gyromagnetic ratio, respectively, defined by $\mu_0 H_k^{eff} = 2K_u^{eff}/M_s$ and $\gamma = g\mu_B/\hbar$, where g, μ_B, and $\hbar$ are Lande's g factor, the Bohr magneton, and Planck's constant, respectively. As shown in Fig. 3, both f and $1/\tau$ are explained well by the LLG equation and the value of α was evaluated to be 0.0089. For the Ta/CoFeB/Ta films, the θ_H dependencies of f and $1/\tau$ are fitted well by Eqs. (3) and (4), and the α values were then evaluated. The results will be shown in Sec. III C.

Figure 4(a) shows the θ_H dependence of f for the case of a 1.0-nm-thick Ta/CoFeB/MgO film that shows PMA at fixed $\mu_0 H_{ext} = 2.01$, 1.58, 1.19, and 0.64 T. Figure 4(b) shows the H_{ext} dependence of f at fixed $\theta_H = 50°$, 65°, and 80°. The solid lines in Figs. 4(a) and 4(b) denote the theoretical f_{LLG} values calculated from Eq. (3) with parameters of $g = 2.01$ and $\mu_0 H_k^{eff} = 0.64$ T, where the values are evaluated by fitting using a fixed $\mu_0 H_{ext}$ of 2.0 T. The evaluated H_k^{eff} is the same as the saturation field that was obtained from the magnetization curve. The K_u^{eff} values shown in Fig. 1(b) were evaluated using the relation of $K_u^{eff} = \mu_0 M_s H_k^{eff}/2$. The M_s values were evaluated based on the magnetization curves and the H_k^{eff} values were obtained from the above analysis.

Figure 5 shows $1/\tau$ obtained from fitting as a function of H_{ext} with different values of $\theta_H = 50°$ (a), 65° (b), and 80° (c). The broken lines in Figs. 5(a)–5(c) are the theoretical values of $1/\tau_{LLG}$ calculated from Eq. (4). The calculated result is quite different to that from the experiments, particularly in the low H_{ext} region, where the difference becomes larger. This is caused by an extrinsic contribution in the low H_{ext} region [27–33]. Therefore, the precession frequency dispersion induced by the anisotropy distribution was considered in the following way, which is similar to the thinking of previous reports using FMR [19,34] and TRMOKE [27,35]. The spatially dependent anisotropy field can be written as $H_k^{eff}(\boldsymbol{r}) = H_k^{eff} + \Delta h_k(\boldsymbol{r})$, where $\Delta h_k(\boldsymbol{r})$ is the deviation of the PMA magnitude from the average value. Then, the spatially dependent precession frequency $\omega(\boldsymbol{r})$ $(=2\pi f)$ and its root-mean-square (rms) $\Delta\omega'$ can be calculated as follows:

$$\omega(\boldsymbol{r}) = \omega_0 + \frac{d\omega_0}{dH_k^{eff}}\Delta h_k(\boldsymbol{r}), \tag{8}$$

$$\Delta\omega' = \sqrt{\langle\omega^2\rangle - \langle\omega\rangle^2} = \left|\frac{d\omega_0}{dH_k^{eff}}\right|\Delta h_k', \tag{9}$$

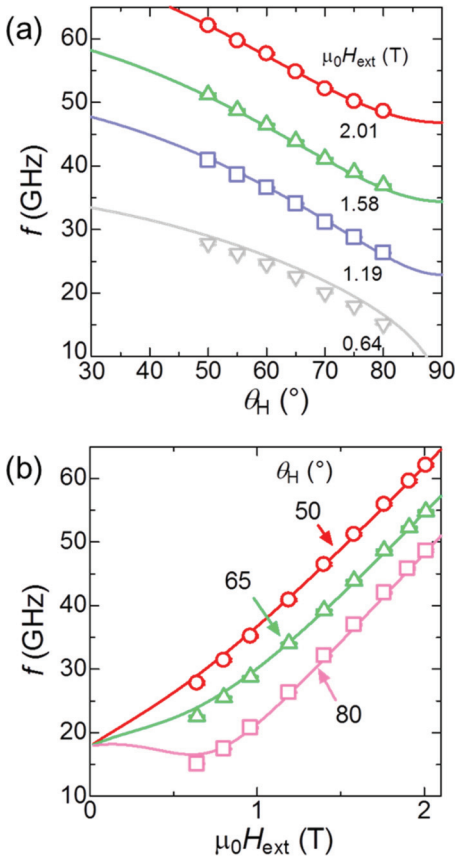

FIG. 4. (Color online) (a) Precession frequency f measured at various external fields H_{ext} plotted as a function of field angle θ_H for the Ta/CoFeB (1.0 nm)/MgO film. This film shows perpendicular magnetic anisotropy. (b) f measured at various values of θ_H as a function of H_{ext}. The solid lines indicate the results of theoretical calculations.

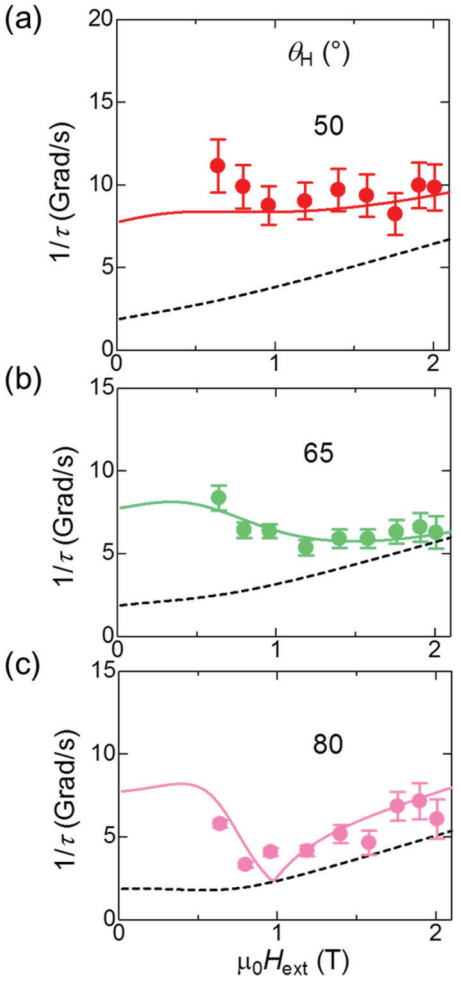

FIG. 5. (Color online) Inverse lifetime $1/\tau$ plotted as a function of H_{ext} for $\theta_H = 50°$ (a), 65° (b), and 80° (c). The solid and broken lines indicate the results of theoretical calculations.

where $\Delta h'_k = \sqrt{\langle \Delta h_k(\boldsymbol{r})^2 \rangle}$ indicates the rms of the PMA field. The inverse lifetime corresponds to the full width at half maximum (FWHM) in the FMR spectrum, because $1/\tau_{calc.} = \Delta\omega_{FWHM}/2$. $\Delta\omega_{FWHM}$ is considered to be a summation of the intrinsic Gilbert damping obtained from Eq. (4) and the frequency dispersion corresponds to Eq. (9) because $\Delta\omega_{FWHM} = \alpha\gamma\mu_0(H_1 + H_2) + 2\sqrt{2\ln 2}\Delta\omega'$. Therefore, $1/\tau_{calc.}$ can be expressed as

$$\frac{1}{\tau_{calc.}} = \frac{1}{2}\alpha\gamma\mu_0(H_1 + H_2) + \sqrt{2\ln 2}\left|\frac{d\omega_0}{dH_k^{eff}}\right|\Delta h'_k. \quad (10)$$

Using two fitting parameters, α and $\Delta h'_k$, we fitted Eq. (10) to all experimental data shown in Figs. 4(a)–4(c). The solid lines in Figs. 5(a)–5(c) are the results of least-squares fitting. The values of α and $\mu_0\Delta h'_k$ were 0.017 and 28 mT, respectively. The details of these values will be discussed in Sec. III C. Here, it should be noted that both the precession frequency and the inverse lifetime obtained from the TRMOKE signals can be explained using the LLG equation while taking only the magnitude dispersion of the magnetic anisotropy into account.

C. Thickness dependence and annealing temperature dependence

Figure 6 shows α as a function of $1/t_{CoFeB}$ with fixed $T_a = 250\,°C$. In the figure, the data reported by other researchers were also plotted. Our Ta/CoFeB/MgO samples with $t_{CoFeB} = 0.8$, 1.0, and 1.2 nm showed perpendicular magnetic anisotropy, while the other samples, including those reported by other researchers, showed in-plane magnetic anisotropy. It is interesting that for both the stacked Ta/CoFeB/Ta and Ta/CoFeB/MgO structures, α is proportional to $1/t_{CoFeB}$, and α for the Ta/CoFeB/Ta samples is larger than that for the Ta/CoFeB/MgO and MgO/CoFeB/Ta samples. This result indicates that the Ta/CoFeB interface enhances α by more than the MgO/CoFeB interface. The enhancement of α for ferro/nonmagnetic interfaces by spin pumping was discussed theoretically and the level of enhancement α' was expressed approximately as [18],

$$\alpha' = \frac{\hbar\gamma}{2\pi M_s}\frac{g^{\uparrow\downarrow}S^{-1}}{t_{CoFeB}}, \quad (11)$$

where $g^{\uparrow\downarrow}$ and S^{-1} denote the mixing conductance and the cross-section area, respectively. The slope of the α vs

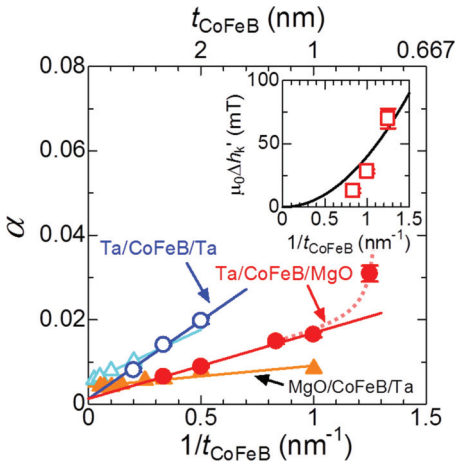

FIG. 6. (Color online) Gilbert damping constant α plotted as a function of the inverse of the CoFeB thickness, $1/t_{CoFeB}$, for Ta/CoFeB/MgO (solid circles) and Ta/CoFeB/Ta (open circles) films. The solid lines indicate the linear relationships and the broken line is intended as a visual guide. The open and solid triangles represent the values obtained from Refs. [37] and [24], respectively. The inset in the figure represents the rms of the PMA field obtained from fitting as a function of $1/t_{CoFeB}$.

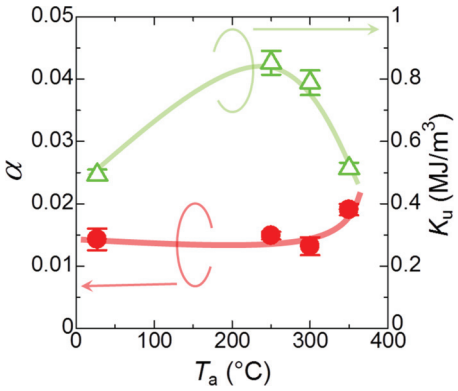

FIG. 7. (Color online) α (solid circles) and K_u (open triangles) as a function of the annealing temperature T_a for the sample where $t_{CoFeB} = 1.2$ nm. The solid lines are intended as visual guides.

$1/t_{CoFeB}$ plot for Ta/CoFeB/Ta is roughly double that of Ta/CoFeB/MgO. This means that α' at the CoFeB/MgO interface is negligibly small when compared with that of the CoFeB/Ta interface. Recently, it was demonstrated that the MgO interface suppresses the spin-pumping effect in MgO/FeB/MgO/Ta structures [36]. The result presented here is consistent with this report. The origin of this enhancement may be related to the mixing conductance $g^{\uparrow\downarrow}$ in Eq. (11).

The solid and open triangles shown in Fig. 6 are the values for the Ta/CoFeB/Ta and MgO/CoFeB/Ta films that were obtained from Refs. [24] and [37], respectively. The slope of the Ta/CoFeB/Ta film in Ref. [37] coincides approximately with that of our results. However, the slope in the case of the MgO/CoFeB/Ta structure in Ref. [24] is much smaller than that in our case. One possible reason for this result is the difference in M_s between the Ta/CoFeB/MgO and MgO/CoFeB/Ta structures. If B or Ta atoms are inside CoFe, the magnetic moment per unit volume will decrease. Also, these atoms work as impurities. In the Elliott-Yafet relaxation mechanism, the spin-flip time that corresponds to the Gilbert damping is proportional to the electron scattering time [14,38]. Therefore, impurities such as B or Ta atoms will cause α to increase. This effect may appear at interfaces like magnetic dead layers. The depth profile showed that more B and Ta atoms exist at the interface [39,40]. Therefore, there is a possibility that the slope is correlated to the concentrations of B or Ta atoms at the interface and that interfacial α may depend on the magnetic moment at the interface. Slight differences in the y intercepts indicate that the α of the bulk may be caused by differences in the CoFeB composition.

The inset of Fig. 6 shows $\Delta h_k'$ obtained from the fitting as a function of $1/t_{CoFeB}$. $\Delta h_k'$ increases dramatically with decreasing t_{CoFeB}. One possible reason for the occurrence of this tendency is the surface roughness, as mentioned in a previous paper [19]. K_u^{eff} shows a linear relationship with $1/t_{CoFeB}$, which originates from the interfacial PMA. Here, the PMA field is considered to be a linear function of $1/t_{CoFeB}$. The solid line in the inset figure is the calculated result using $\Delta h_k' = H_i/t_{CoFeB}^2 \cdot \sqrt{\langle t_{CoFeB}^2\rangle - \langle t_{CoFeB}\rangle^2}$, where the rms roughness is assumed to be the same with a thickness dispersion of 0.02 nm and an interfacial PMA field $\mu_0 H_i$ of 2 T nm were used. The roughness model can roughly explain the change in the anisotropy dispersion.

Figure 7 shows α and K_u as functions of the annealing temperature T_a with fixed $t_{CoFeB} = 1.2$ nm. K_u shows a broad maximum at approximately $T_a = 250\sim300$ °C. This behavior may be explained by CoFeB crystallization, corresponding to an increase in K_u and diffusion of the Ta atoms into CoFeB, corresponding to a reduction in K_u. Although K_u depends on T_a, α does not depend significantly on T_a. In the cases of Co/Pd and CoFe/Pd multilayers, it was shown that α was not correlated with the PMA value, and that the spin-pumping effect enhanced α [41,42]. Also, in the case of Ta/CoFeB/MgO thin films, PMA and α are not found to be correlated in this paper. This result means that by controlling the interfaces between the magnetic and nonmagnetic layers, we can fabricate materials with low α and high PMA.

IV. CONCLUSION

We investigated the precession frequency f and the lifetime τ as functions of magnetic field strength and applied field direction for both Ta/CoFeB/MgO and Ta/CoFeB/Ta films. These data were analyzed using the LLG equation. For the films with $t_{CoFeB} > 2.0$ nm, f and $1/\tau$ were fitted well using the LLG equations and the α values were evaluated uniquely. For films with $t_{CoFeB} < 1.2$ nm, which exhibited perpendicular magnetic anisotropy, the α values were evaluated by taking the magnetic anisotropy dispersion into account. α was proportional to $1/t_{CoFeB}$ for both the Ta/CoFeB/Ta and Ta/CoFeB/MgO films. The values of α for the former stacks were larger than those for the latter stacks, while perpendicular magnetic anisotropy could only be achieved in the latter case. No correlation between α and the perpendicular magnetic anisotropy constant K_u was found.

ACKNOWLEDGMENTS

This work was supported in part through a Grant for Industrial Technology Research from NEDO (Grant No. 11B07010d), a Grant-in-Aid for Scientific Research from the JSPS (Grant No. 24686001), support from the Asahi Glass Foundation, and research funding under "Grants for Excellent Graduate Schools."

[1] J. C. Slonczewski, J. Magn. Magn. Mater. **159**, L1 (1996).
[2] S. Ikeda, J. Hayakawa, Y. Ashizawa, Y. M. Lee, K. Miura, H. Hasegawa, M. Tsunoda, F. Matsukura, and H. Ohno, Appl. Phys. Lett. **93**, 082508 (2008).
[3] H. D. Gan, H. Sato, M. Yamanouchi, S. Ikeda, K. Miura, R. Koizumi, F. Matsukura, and H. Ohno, Appl. Phys. Lett. **99**, 252507 (2011).
[4] S. Ikeda, K. Miura, H. Yamamoto, K. Mizunuma, H. D. Gan, M. Endo, S. Kanai, J. Hayakawa, F. Matsukura, and H. Ohno, Nat. Mater. **9**, 721 (2010).
[5] H. X. Yang, M. Chshiev, B. Dieny, J. H. Lee, A. Manchon, and K. H. Shin, Phys. Rev. B **84**, 054401 (2011).
[6] C.-W. Cheng, W. Feng, G. Chern, C. M. Lee, and T.-h. Wu, J. Appl. Phys. **110**, 033916 (2011).
[7] H. Meng, W. H. Lum, R. Sbiaa, S. Y. H. Lua, and H. K. Tan, J. Appl. Phys. **110**, 033904 (2011).
[8] M. Yamanouchi, R. Koizumi, S. Ikeda, H. Sato, K. Mizunuma, K. Miura, H. D. Gan, F. Matsukura, and H. Ohno, J. Appl. Phys. **109**, 07C712 (2011).
[9] S. Ikeda, R. Koizumi, H. Sato, M. Yamanouchi, K. Miura, K. Mizunuma, H. Gan, F. Matsukura, and H. Ohno, IEEE Trans. Magn. **48**, 3829 (2012).
[10] W. X. Wang, Y. Yang, H. Naganuma, Y. Ando, R. C. Yu, and X. F. Han, Appl. Phys. Lett. **99**, 012502 (2011).
[11] D. D. Lam, F. Bonell, S. Miwa, Y. Shiota, K. Yakushiji, H. Kubota, T. Nozaki, A. Fukushima, S. Yuasa, and Y. Suzuki, J. Magn. **18**, 5 (2013).
[12] M. Oogane, T. Wakitani, S. Yakata, R. Yilgin, Y. Ando, A. Sakuma, and T. Miyazaki, Jpn. J. Appl. Phys. **45**, 3889 (2006).
[13] A. Conca, J. Greser, T. Sebastian, S. Klingler, B. Obry, B. Leven, and B. Hillebrands, J. Appl. Phys. **113**, 213909 (2013).
[14] V. Kambersky, Can. J. Phys. **48**, 2906 (1970).
[15] P. Bruno, Phys. Rev. B **39**, 865 (1989).
[16] S. Mizukami, E. P. Sajitha, D. Watanabe, F. Wu, T. Miyazaki, H. Naganuma, M. Oogane, and Y. Ando, Appl. Phys. Lett. **96**, 152502 (2010).
[17] E. Barati, M. Cinal, D. M. Edwards, and A. Umerski, EPJ Web Conf. **40**, 18003 (2013).
[18] Y. Tserkovnyak, A. Brataas, and G. E. W. Bauer, Phys. Rev. B **66**, 224403 (2002).
[19] S. Mizukami, Y. Ando, and T. Miyazaki, Jpn. J. Appl. Phys. **40**, 580 (2001).
[20] J. Lindner, I. Barsukov, C. Raeder, C. Hassel, O. Posth, R. Meckenstock, P. Landeros, and D. L. Mills, Phys. Rev. B **80**, 224421 (2009).
[21] N. Mo, J. Hohlfeld, M. Islam, C. S. Brown, E. Girt, P. Krivosik, W. Tong, A. Rebei, and C. E. Patton, Appl. Phys. Lett. **92**, 022506 (2008).
[22] H. Lee, Y.-H. A. Wang, C. K. A. Mewes, W. H. Butler, T. Mewes, S. Maat, B. York, M. J. Carey, and J. R. Childress, Appl. Phys. Lett. **95**, 082502 (2009).
[23] S. Iihama, Q. L. Ma, T. Kubota, S. Mizukami, Y. Ando, and T. Miyazaki, Appl. Phys. Express **5**, 083001 (2012).
[24] X. Liu, W. Zhang, M. J. Carter, and G. Xiao, J. Appl. Phys. **110**, 033910 (2011).
[25] T. Devolder, P.-H. Ducrot, J.-P. Adam, I. Barisic, N. Vernier, Joo-Von Kim, B. Ockert, and D. Ravelosona, Appl. Phys. Lett. **102**, 022407 (2013).
[26] S. Mizukami, F. Wu, A. Sakuma, J. Walowski, D. Watanabe, T. Kubota, X. Zhang, H. Naganuma, M. Oogane, Y. Ando, and T. Miyazaki, Phys. Rev. Lett. **106**, 117201 (2011).
[27] G. Malinowski, K. C. Kuiper, R. Lavrijsen, H. J. M. Swagten, and B. Koopmans, Appl. Phys. Lett. **94**, 102501 (2009).
[28] S. Mizukami, S. Iihama, N. Inami, T. Hiratsuka, G. Kim, H. Naganuma, M. Oogane, and Y. Ando, Appl. Phys. Lett. **98**, 052501 (2011).
[29] S. Mizukami, D. Watanabe, T. Kubota, X. Zhang, H. Naganuma, M. Oogane, Y. Ando, and T. Miyazaki, Appl. Phys. Express **3**, 123001 (2010).
[30] H-S. Song, K-D. Lee, J-W. Sohn, S-H. Yang, S. S. P. Parkin, C-Y. You, and S-C. Shi, Appl. Phys. Lett. **102**, 102401 (2013).
[31] J. Walowski, M. D. Kaufmann, B. Lenk, C. Hamann, J. McCord, and M. Munzenberg, J. Phys. D **41**, 164016 (2008).
[32] A. J. Schellekens, L. Deen, D. Wang, J. T. Kohlhepp, H. J. M. Swagten, and B. Koopmans, Appl. Phys. Lett. **102**, 082405 (2013).
[33] T. Kato, Y. Matsumoto, S. Okamoto, N. Kikuchi, O. Kitakami, N. Nishizawa, S. Tsunashima, and S. Iwata, IEEE Trans. Magn. **47**, 3036 (2011).
[34] R. D. McMichael, J. Appl. Phys. **95**, 7001 (2004).
[35] S. Mizukami, D. Watanabe, T. Kubota, X. Zhang, H. Naganuma, M. Oogane, Y. Ando, and T. Miyazaki, IEEE Trans. Magn. **47**, 3897 (2011).
[36] M. Konoto, H. Imamura, T. Taniguchi, K. Yakushiji, H. Kubota, A. Fukushima, K. Ando, and S. Yuasa, Appl. Phys. Express **6**, 073002 (2013).
[37] H. Lee, L. Wen, M. Pathak, P. Janssen, P. LeClair, C. Alexander, C. K. A. Mewes, and T. Mewes, J. Phys. D **41**, 215001 (2008).
[38] R. J. Elliott, Phys. Rev. **96**, 266 (1954).
[39] T. Zhu, Y. Yang, R. C. Yu, H. Ambeya, V. Lauter, and J. Q. Xiao, Appl. Phys. Lett. **100**, 202406 (2012).
[40] N. Miyakawa, D. C. Worledge, and K. Kita, IEEE Magn. Lett. **4**, 1000104 (2013).
[41] T. Kato, Y. Matsumoto, S. Kashima, S. Okamoto, N. Kikuchi, S. Iwata, O. Kitakami, and S. Tsunashima, IEEE Trans. Magn. **48**, 3288 (2012).
[42] J. M. Shaw, H. T. Nembach, and T. J. Silva, Phys. Rev. B **85**, 054412 (2012).